Economic Geology, v. 108, pp. 1849–1864

PGE and Isotope (Hf-Sr-Nd-Pb) Constraints on the Origin of the Huangshandong Magmatic Ni-Cu Sulfide Deposit in the Central Asian Orogenic Belt, Northwestern China

Tao Sun,[1] Zhuang-Zhi Qian,[1,†] Yu-Feng Deng,[2] Chusi Li,[3] Xie-Yan Song,[4] and Qingyan Tang[5]

[1] *MOE Key Laboratory of Western China Mineral Resources and Geological Engineering, College of Earth Sciences and Resources, Chang'an University, Xi'an 710054, China*

[2] *School of Natural Resources and Environmental Engineering, Hefei University of Technology, Hefei*

[3] *Department of Geological Sciences, Indiana University, Bloomington, Indiana 47405*

[4] *State Key Laboratory of Ore Deposit Geochemistry, Institute of Geochemistry, Chinese Academy of Sciences, Guiyang 550002, China*

[5] *School of Earth Sciences, Lanzhou University, Gansu 730000, China*

Abstract

Many magmatic Ni-Cu sulfide deposits have been found to be associated with Permian basaltic magmatism in the Central Asian orogenic belt, Xinjiang, China. The style of basaltic magmatism and the origin of associated Ni-Cu sulfide deposits in the region are highly debated. The Huangshandong mafic-ultramafic intrusion is at the center of the debate mainly because it hosts the largest magmatic Ni-Cu sulfide deposit in the region. In this paper we report integrated petrological and geochemical data for the Huangshandong Ni-Cu sulfide deposit. The host intrusion consists of a massive gabbronorite unit and a layered sequence, which is composed of two to three ultramafic layers overlain by gabbroic rocks with visible modal layering. Important sulfide mineralization in the intrusion is associated with the ultramafic rocks and massive gabbronorite. The ultramafic rocks and massive gabbronorite are characterized by moderate enrichments in light rare earth elements (LREE), pronounced negative Nb-Ta anomalies relative to Th and La, positive ε_{Nd} (t = 274 Ma) values (6.6–8.3), low initial $^{87}Sr/^{86}Sr$ ratios (0.7031–0.7038), low initial $^{206}Pb/^{204}Pb$ ratios (17.7–18), and positive ε_{Hf} values of zircon (14–17). These data are consistent with mixing between a depleted mantle-derived magma and a granitic melt formed by partial melting of a juvenile arc crust as a result of mafic magma underplating. Olivine crystals enclosed in large clinopyroxene and plagioclase crystals from the ultramafic rocks have Fo contents up to 83 mol %. The contents of Ni in the olivine crystals decrease rapidly with Fo contents, indicating sulfide segregation from magma during olivine crystallization. Numerical modeling using bulk sulfide compositions and constraints from olivine-liquid relationships reveals that the parental magma of the intrusion was significantly depleted in PGE and contained <7 wt % MgO. Depletion of PGE in the magma can be explained by previous sulfide segregation possibly due to magma mixing in a staging chamber. Fractional crystallization and addition of external sulfides from juvenile arc crust appear to have played a critical role in triggering the second event of sulfide segregation to form the deposit. We believe that the Huangshandong sulfide ore-bearing intrusion formed by basaltic magmatism related to postsubduction delamination and asthenosphere upwelling instead of a deep-seated mantle plume.

Introduction

Several decades of persistent, state-funded exploration activities in northern Xinjiang have led to the discovery of several important clusters of Ni-Cu deposits hosted by small mafic-ultramafic intrusions in the southern margin of the Central Asian orogenic belt (Fig. 1a). The most important one is the East Tianshan nickel belt in which more than 10 small magmatic sulfide deposits of Permian ages have been found to date (Fig. 1b). Nickel mining, which started ~15 years ago, is still active in the region. Meanwhile, the state-funded Ni exploration program, which started two decades ago, is running stronger than ever in terms of total budget. This region is currently viewed by the Chinese government to have great potential for new discoveries of magmatic Ni-Cu sulfide deposits.

The Huangshandong deposit was described in Chinese literature about two decades ago (Wang et al., 1987; Li et al., 1989; Mao et al., 2003). It contains >50 million metric tons (Mt) sulfide ores with 0.52 wt % Ni and 0.27 wt % Cu (Wang et al., 1987). Han et al. (2004) were the first to report a zircon U-Pb age (274 ± 3 Ma by SHRIMP) for the deposit. Zhou et al. (2004) were the first to introduce the deposit to international readers. These authors suggested that the Huangshandong mafic-ultramafic intrusion has a tholeiitic affinity. In contrast, Xiao et al. (2009) regarded it as an Alaska-type intrusion. After the discovery of Permian alkaline basalts in the Tarim basin a few years ago (Fig. 1), some researchers suggested that the Permian mafic-ultramafic intrusions, including the Huangshandong intrusion in the southern part of the Central Asian orogenic belt and the Tarim alkaline basalts, belong to a single mantle plume (e.g., Zhou et al., 2009; Qin et al., 2011; Su et al., 2011). This view has been challenged by other researchers who believe that the mafic-ultramafic intrusions formed by basaltic magmatism related to postsubduction delamination and asthenosphere upwelling (e.g., Song et al., 2011; Tang et al., 2011; Zhang, M., et al., 2011; Li et al., 2012a). The Huangshandong intrusion, which hosts the largest magmatic Ni-Cu sulfide deposit in the region, has always been at the center of this debate. However, no systematic petrological, and geochemical studies of this deposit have been reported in international journals. In this paper, we present integrated mineralogical, petrological and isotopic data for the deposit. We use these data to evaluate the source mantle characteristics, tectonomagmatic affinity, and genetic

† Corresponding author: email, zyxyqzz8@chd.edu.cn

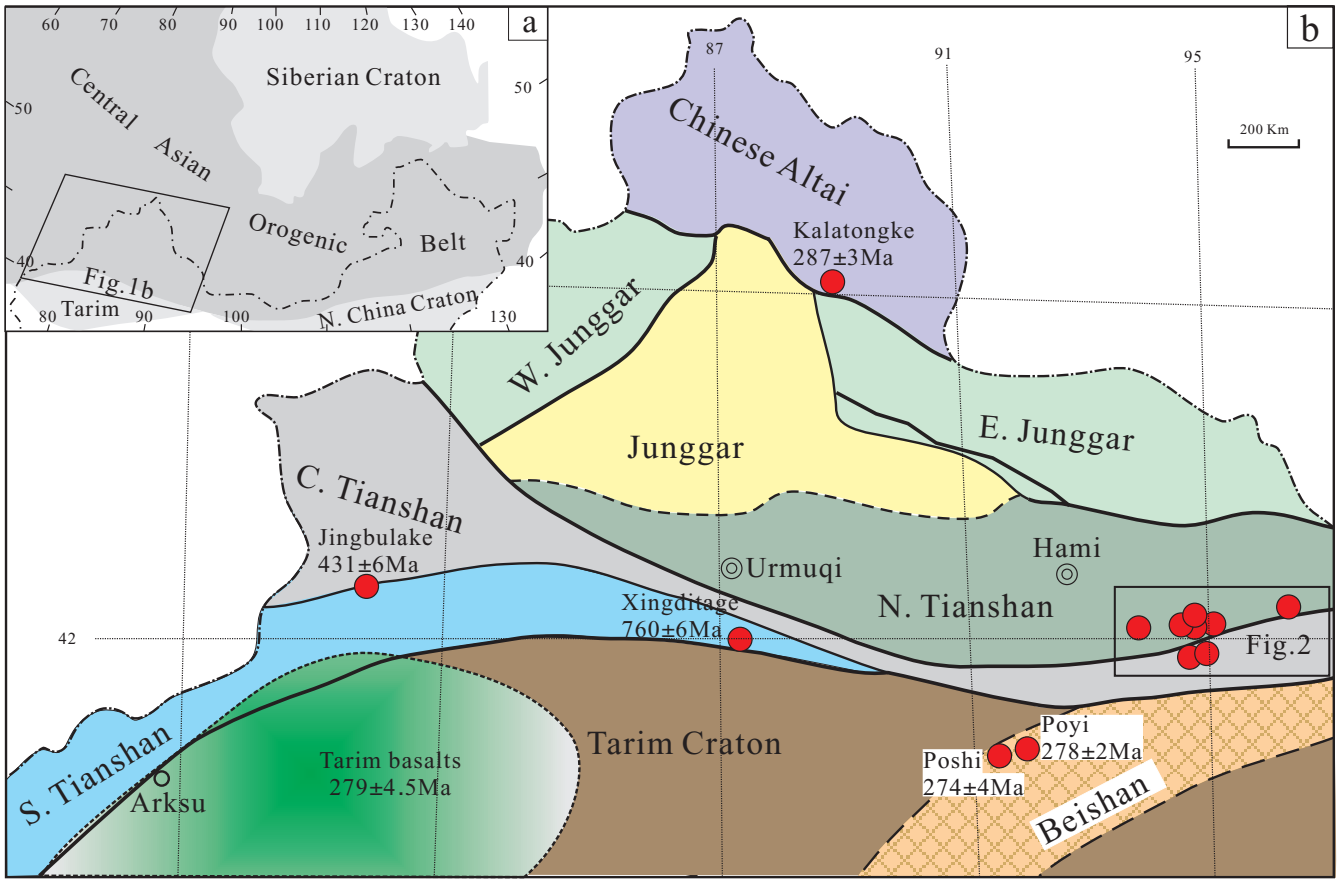

FIG. 1. Outline of the Central Asian orogenic belt (a) and distribution of magmatic Cu-Ni sulfide deposits and/or showings in northern Xinjiang (b). Zircon U-Pb ages: Kalatongke (Han et al., 2004), Jingbulake (Yang and Zhou, 2009), Xingditage (Zhang, C.-L., et al., 2011), Poshi (Jiang et al., 2006), Poyi (Li et al., 2006), Tarim alkaline basalts (Tian et al., 2010).

relationship between magma evolution and sulfide mineralization in the Huangshandong magmatic system.

Geologic Background

The Chinese Tianshan orogenic belts are located in the southern part of the Central Asian orogenic belt, which formed by amalgamation of microcontinents and arc accretion (Jahn, 2004) prior to the Early Permian (e.g., Wang et al., 2010) or Early Triassic (e.g., Xiao et al., 2003). The boundaries of the subparallel orogenic belts are marked by ophiolites of pre-Permian ages, regional faults, and high-grade metamorphic rocks (e.g., Xiao et al., 2004). Topographically they form prominent E-W-trending mountain ranges. From south to north, they are named South Tianshan, Central Tianshan, and North Tianshan. South Tianshan is only present in the west (Fig. 1b). The eastern parts of Central Tianshan and North Tianshan are collectively referred to as East Tianshan in the literature. East Tianshan is the southernmost part of the Central Asian orogenic belt (Fig. 1b). It is bounded by the Tarim craton to the south. Numerous small, sulfide-mineralized mafic-ultramafic intrusions with similar ages occur across the boundary between these two different tectonic units (Fig. 1b).

In East Tianshan, the most important magmatic sulfide deposits are of Early Permian age and occur in the Jueluotage terrane, one of several NE-trending, fault-bounded terranes of the North Tianshan orogenic belt (Fig. 2). On the surface the long axes of the Permian mafic-ultramafic intrusions in the Huangshan nickel belt, including the Huangshandong intrusion, are generally subparallel to regional structural lineaments (Fig. 3a), which has been used as evidence for magma emplacement during regional dextral shearing by some researchers (e.g., Branquet et al., 2012). Many A-type granite plutons of Paleozoic age are present in East Tianshan. Some of them are contemporaneous with the sulfide-mineralized mafic-ultramafic intrusions in the region (e.g., Yuan et al., 2010). Early Permian bimodal volcanic rocks (basalt-rhyolite) are found in the eastern parts of the North Tianshan orogenic belt (Zhou et al., 2006; Shu et al., 2011).

Petrology and Petrography

The Huangshandong Ni-Cu sulfide deposit is hosted in a mafic-ultramafic intrusion which intruded Mesoproterozoic biotite schists and amphibolites. On the surface it has an oval shape, measuring ~3.5 km in length and ~1.2 km in width (Fig. 3a). A keel is present at the west end (Fig. 3b). The rest of the intrusion has a funnel shape (Fig. 3c). The downward extension of intrusion exceeds 1,000 m in the central part (Fig. 3b). The intrusion can be divided into a massive gabbronorite unit, a layered sequence and a marginal diorite zone surrounding the layered sequence in some places (Fig. 3a). The layered sequence is composed of two to three upward concave layers of ultramafic rocks overlain by olivine gabbro,

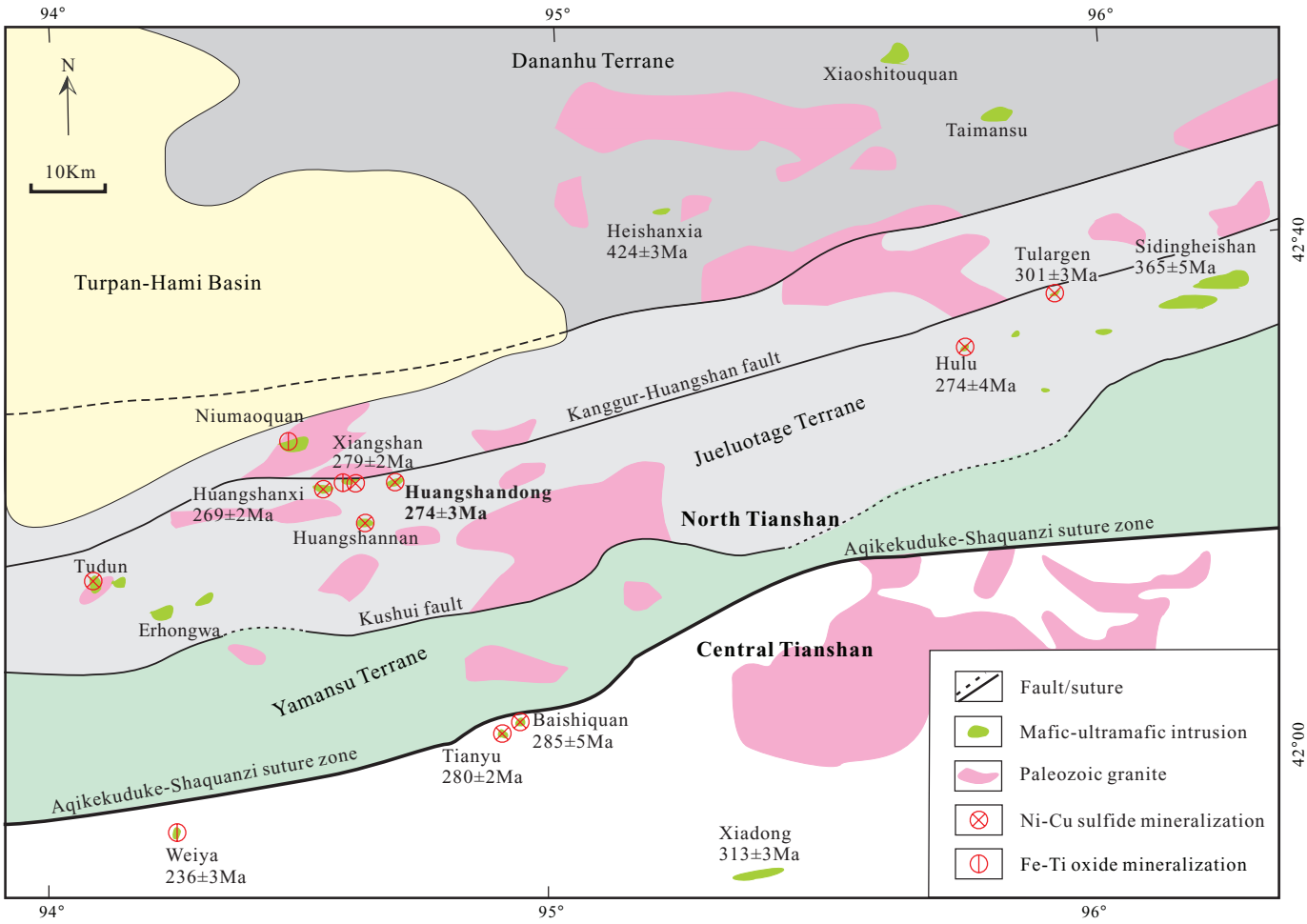

FIG. 2. Simplified regional geologic map of East Tianshan and distribution of magmatic Ni-Cu deposits in the region. Zircon U-Pb ages: Huangshandong (Han et al., 2004), Huangshanxi (Zhou et al., 2004), Weiya (Wang et al., 2008), Xiangshan (Xiao et al., 2010), Hulu (Sun et al., 2010), Tulargen (San et al., 2010), Tianyu (Tang et al., 2011), Heishanxia, Sidingheishan, and Baishiquan (Su et al., 2011), Xiadong (Su et al., 2012).

gabbro, and gabbrodiorite (Fig. 3b). Modal layering is visible in the outcrops of the gabbroic sequence. The ultramafic rocks are lherzolite, wehrlite, and olivine websterlite. In the western part of the intrusion the layered sequence was intruded by the gabbronorite unit (Fig. 3b). The contacts between the gabbronorite unit and the layered sequence are sharp but no chilled margins are observed between them.

The most important sulfide ores of the Huangshandong Ni-Cu deposit are disseminated and net-textured sulfides. Massive sulfide ores are insignificant. The sulfide mineralization mainly occurs in its western part as small lenses or irregular zones, predominantly associated with the ultramafic rocks of the layered sequence and the massive gabbronorite unit, rarely with the gabbroic rocks of the layered sequence (Fig. 3b). Multiple sulfide lenses occur within the upper ultramafic layer (Fig. 3c). In each of these sulfide-mineralized lenses the abundance of sulfides tends to decrease upward. In contrast, no systematic spatial variation in sulfide abundance is present in the sulfide-mineralized zones associated with the lower ultramafic layer and the gabbronorite unit.

In the ultramafic rocks, olivine crystals enclosed in clinopyroxene (Fig. 4a), plagioclase (Fig. 4b), and orthopyroxene are generally unaltered, and those in direct contact with sulfides are more commonly altered to serpentine plus secondary magnetite. In the gabbronorite unit, hydrothermal alteration is generally more pronounced in the sulfide-bearing samples than in the sulfide-poor samples. Gabbro and diorite away from fault zones are generally unaltered. The most common alteration minerals in the mafic rocks are tremolite after clinopyroxene, talc after orthopyroxene, and chlorite + epidote + albite after plagioclase.

Pyrrhotite, pentlandite, and chalcopyrite are the major phases of the sulfide ores in the Huangshandong intrusion (Fig. 4c-d). Sperrylite is the most important platinum group mineral (PGM) found to date (Wang et al., 1987). The $\delta^{34}S$ values of sulfides from the Huangshandong Ni-Cu deposit vary between –0.8 and +2.8‰ (Wang et al., 1987). The average γ_{Os} value of the sulfide ores is ~100 (Mao et al., 2003).

Analytical Methods

Mineral compositions were determined by wavelength-dispersive X-ray analysis using an EPMA-8100 electron microprobe at Chang'an University, Xi'an, China. The analytical conditions were 15-kV, 20-nA beam current, 1-μm beam size,

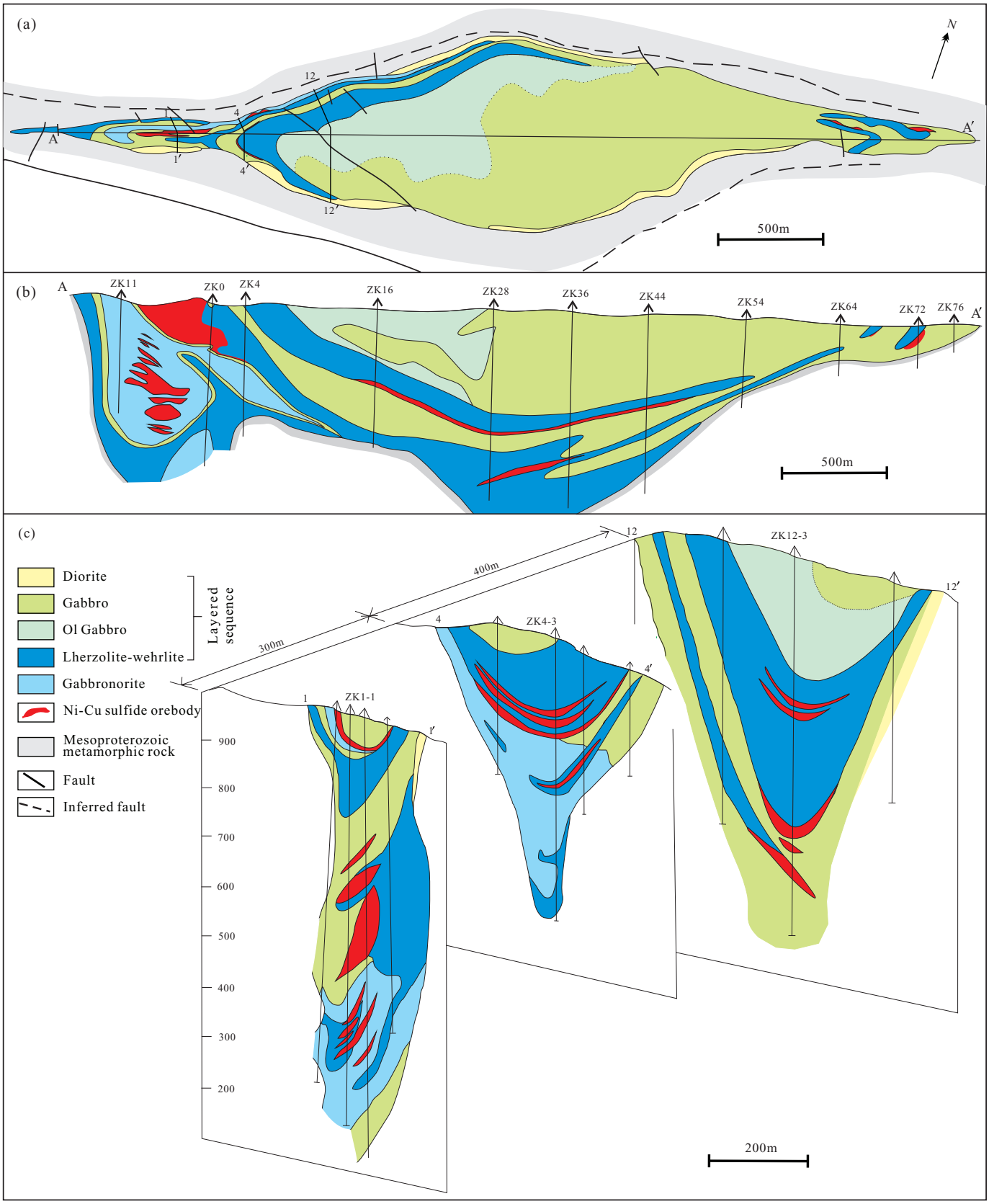

FIG. 3. Plan view (a), long section (b), and cross sections (c) of the Huangshandong sulfide ore-bearing mafic-ultramafic intrusion (after Li et al., 1989). Ol = olivine.

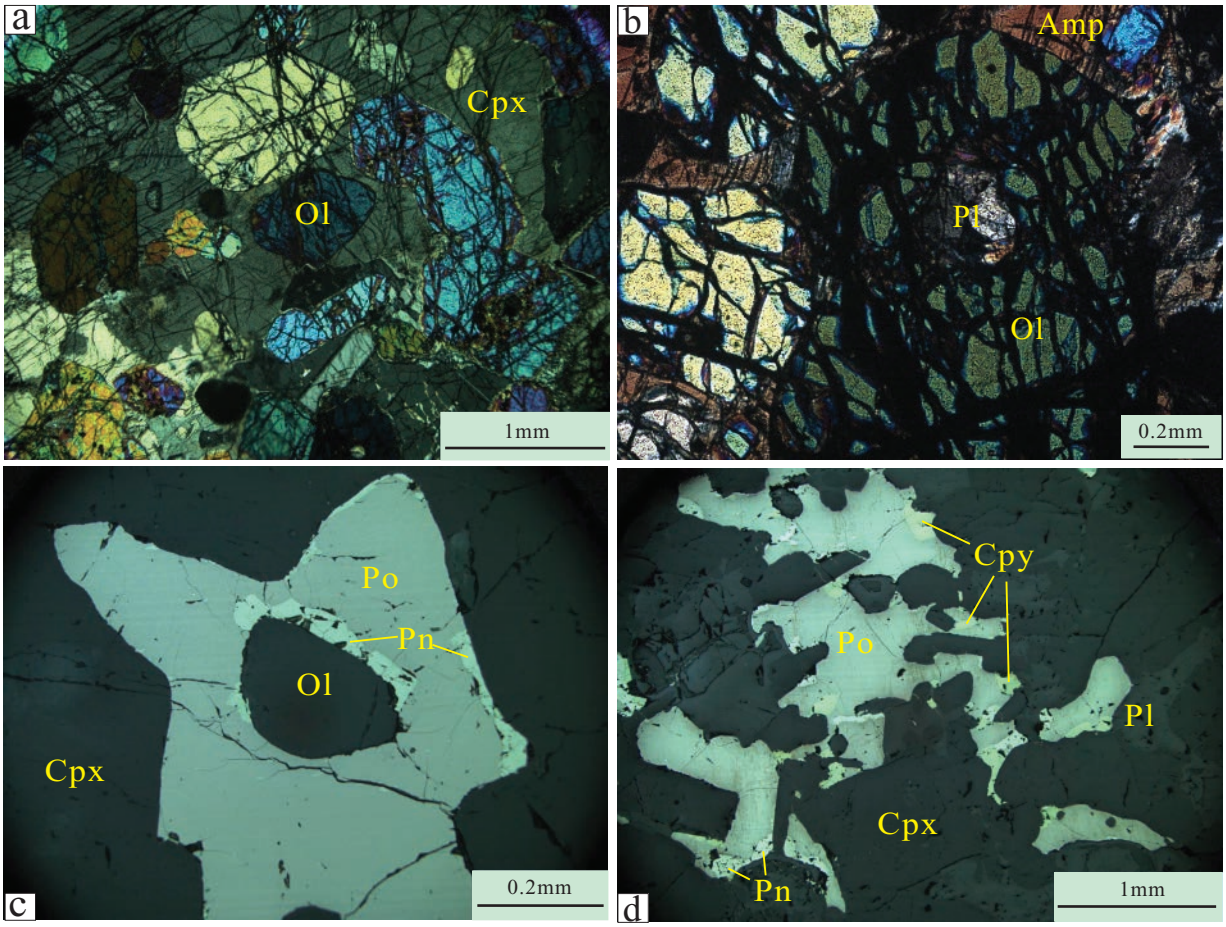

FIG. 4. Microphotographs of important rock and sulfide textures of the Huangshandong sulfide ore-bearing intrusion. (a). Wehrlite with a poikilitic texture characterized by small olivine crystals enclosed in large clinopyroxene crystals. (b). A small plagioclase crystal enclosed in a large olivine crystal in plagioclase-bearing lherzolite. (c). Interstitial sulfides in wehrlite. (d). Interstitial sulfides in gabbronorite. Abbreviations: Amp = amphibole, Cpx = clinopyroxene, Cpy = chalcopyrite, Ol = olivine, Opx = orthopyroxene, Pl = Plagioclase, Po = pyrrhotite, Pn = pentlandite.

and peak counting time of 20 s for major elements. Nickel in olivine was analyzed using a beam current of 80 nA and a peak counting time of 50 s. The detection limit for Ni under these conditions is ~100 ppm. Analytical reproducibility was within 2%. The accuracy of olivine analysis was monitored using the San Carlo olivine standard.

Whole-rock major elements were determined by XRF in the National Research Center of Geoanalysis in Beijing, China. Whole-rock trace element compositions were determined by acid digestion in steel-jacketed Teflon "bombs" followed by analysis by inductively coupled plasma-mass spectrometry (ICP-MS) at Chang'an University, Xi'an, China. Sulfur concentrations in whole rocks were determined using a Vario EL2 elemental analyzer. The concentrations of PGE in sulfide-mineralized samples were determined by the combination of NiS bead preconcentration and Te coprecipitation, followed by ICP-MS analysis at Guangzhou Institute of Geochemistry, Chinese Academy of Sciences. The concentrations of PGE in sulfide-poor samples were determined by Carius tube digestion isotope dilution, followed by ICP-MS analysis at Chang'an University, Xi'an, China. The detailed analytical procedures, blank concentrations, and detection limits are given in Sun and Sun (2005) and Sun et al. (2009).

Whole-rock Sr-Nd-Pb isotope analyses were carried out at Guangzhou Institute of Geochemistry, Chinese Academy of Sciences. Rb-Sr and Sm-Nd isotopes were determined using MC-ICP-MS, the procedural blanks were ~10 pg for Sm and Nd, and ~20 pg for Rb and Sr. The measured values for the LaJolla Nd standard and the SRM987 Sr standard were $^{143}Nd/^{144}Nd = 0.511861 \pm 10$ and $^{87}Sr/^{86}Sr = 0.710263 \pm 10$ during the period of data acquisition. Pb isotopes were determined using VG354 thermal ionization mass spectrometry (TIMS), the procedural blanks were ~100 pg. The measured values for the SRM981 Pb standard were $^{206}Pb/^{204}Pb = 16.934 \pm 0.007$, $^{207}Pb/^{204}Pb = 15.486 \pm 0.017$, and $^{208}Pb/^{204}Pb = 36.673 \pm 0.033$ ($n = 20$), respectively.

Hf isotopes in zircon crystals were determined in situ, by using laser ablation-multiple collectors-inductively coupled plasma-mass spectrometry (LA-MC-ICP-MS) analysis at the State Key Laboratory of Continental Dynamics, Northwest University, Xi'an, China. Euhedral, colorless, and transparent zircon crystals were selected for the analysis. The selected grains were mounted in an epoxy resin disk and then polished, cleaned, and carbon coated. Before analysis, individual grains were photographed under both transmitted and reflected light, and examined for zoning using cathodoluminescence

imaging. The grains with striped absorption and clear oscillatory zoning were selected for Hf isotope analysis. The detailed analytical procedures can be found in Yuan et al. (2008). Repeat analyses of zircon standards 91500 and GJ-1 during the course of sample analysis gave consistent results within the certified range for these standards, 0.282307 ± 0.000031(2σ) and 0.282015 ± 0.000019 (2σ), respectively.

Analytical Results

Olivine chemistry

The average compositions of olivine crystals enclosed in pyroxene and plagioclase in the Huangshandong ultramafic rocks are given in the Appendix (Table A1). The maximum average Fo content of olivine from this intrusion is ~82 mol %, about 4 mol % less than the maximum value of olivine from the nearby Huangshanxi sulfide ore-bearing intrusion (see Fig. 2). Compared to olivine crystals with the same Fo contents from the Huangshanxi intrusion, the contents of Ni in olivine crystals from the Huangshandong intrusion are higher by up to 1000 ppm (Fig. 5). In addition, the contents of Ni in olivine crystals decrease more rapidly with decreasing Fo contents in the Huangshandong intrusion than in the Huangshanxi intrusion. Compared to olivine in the ultramafic rocks of the Huangshandong intrusion, olivine in the associated gabbroic rocks is more fractionated (i.e., lower Fo contents) and significantly depleted in Ni (Fig. 5).

Major and trace elements

Whole-rock major and trace element compositions of the Huangshandong intrusion are given in the Appendix (Table A2). The chondrite-normalized REE and primitive mantle-normalized immobile trace element patterns for the Huangshandong ultramafic rocks and gabbronorites are illustrated in Figure 6. In these plots, the average compositions of Permian basalts and coeval mafic-ultramafic dikes in the Tarim craton, and global volcanic arc basalts are included for comparison. The Huangshandong ultramafic rocks are characterized by low REE abundances and moderate light REE enrichments relative to heavy REE (Fig. 6a). The Huangshandong gabbronorites are also characterized by moderate light REE enrichments, higher REE abundances than the associated ultramafic rocks, and significant positive Eu anomalies (Fig. 6c). Unlike Permian mafic-ultramafic volcanic and intrusive rocks in the Tarim craton, the Permian Huangshandong intrusion in the Central Asian orogenic belt shows pronounced negative Nb-Ta anomalies relative to Th and La (Fig. 6b, d). The Th/Yb and Nb/Yb ratios of the Huangshandong intrusive rocks are different from that of Permian mafic-ultramafic volcanic and intrusive rocks in the Tarim craton but similar to those of the global volcanic arc basalts (Fig. 7). The Huangshandong intrusion has lower Nb/Yb ratios than that of typical Alaska-type intrusions.

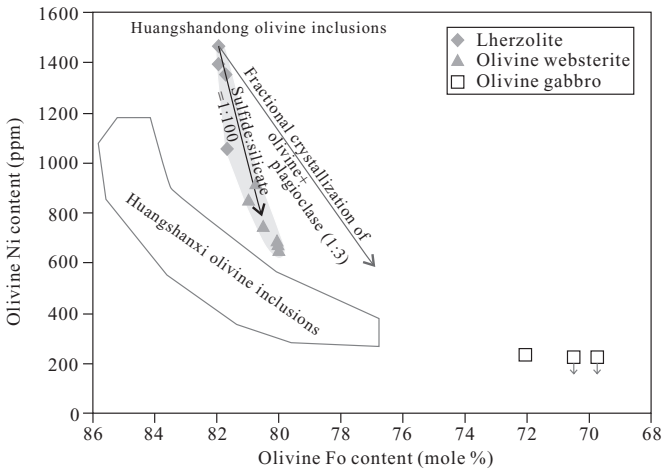

FIG. 5. Plot of Ni vs. Fo of olivine crystals enclosed in clinopyroxene or plagioclase in sulfide-poor samples. Data for the Huangshandong intrusion are from this study. Data for the Huangshanxi intrusion are from M. Zhang et al. (2011). See text for modeling.

Ni, Cu, and platinum group elements (PGE)

The concentrations of PGE, Cu, Ni, and S in both sulfide-poor (no visible sulfide in hand specimen) and sulfide-bearing samples, including ore samples from the Huangshandong intrusion, are given in Table 1. The relationships between some chalcophile elements and S in the samples analyzed by us plus those analyzed by Gao et al. (2013) are illustrated in Figure 8. All the data together show good positive correlation between Ir and S (Fig. 8b), weak positive correlations between Ni, Pd, and S (Fig. 8c-d), and no correlation between Pt and S (Fig. 8d). The data from both studies collectively also indicate weak correlations between Os, Ru, and S and no correlation between Cu and S. However, our data alone show there is a weak positive correlation between Pt and S (Fig. 8d).

The primitive mantle-normalized patterns of Cu, Ni, and PGE for sulfide-poor samples, sulfide-bearing samples, and massive sulfide ores are illustrated in Figure 9. The sulfide-bearing rocks and massive sulfide ores have much higher PGE abundances than the sulfide-poor samples. The massive sulfide ores also show significant depletions of PGE relative to Cu and Ni. The depletions are also present in most of the other samples.

Hf-Sr-Nd-Pb isotopes

The Hf isotope compositions of 26 zircon crystals separated from a large gabbroic sample from the layered sequence of the Huangshandong intrusion are listed in Table 2. The calculated ε_{Hf} (t = 274 Ma) values of zircons from the Huangshandong intrusion vary from 14 to 17. These values are slightly higher than that of zircons from Permian A-type granites but within the range of zircons from other Permian mafic-ultramifin intrusions in the region such as the Xiangshan and Huangshanxi intrusions (Fig. 10).

Whole-rock Sr, Nd, and Pb isotope compositions of the Huangshandong intrusion are listed in Table 3. The calculated ε_{Nd} (t = 274 Ma) values and initial $^{87}Sr/^{86}Sr$ ratios are between 6.6 and 8.3, and between 0.7031 and 0.7038, respectively (Fig. 11a). The calculated initial $^{206}Pb/^{204}Pb$ values vary narrowly between 17.7 and 18.0. The Sr-Nd isotope compositions of the Huangshandong intrusion are significantly different from that of Permian basalts and coeval mafic-ultramafic dikes in the Tarim basin (Fig. 11b). The Huanhshandong samples plot between the fields of midocean ridge basalt (MORB) and global volcanic arc basalts, overlapping with both fields (Fig. 11b).

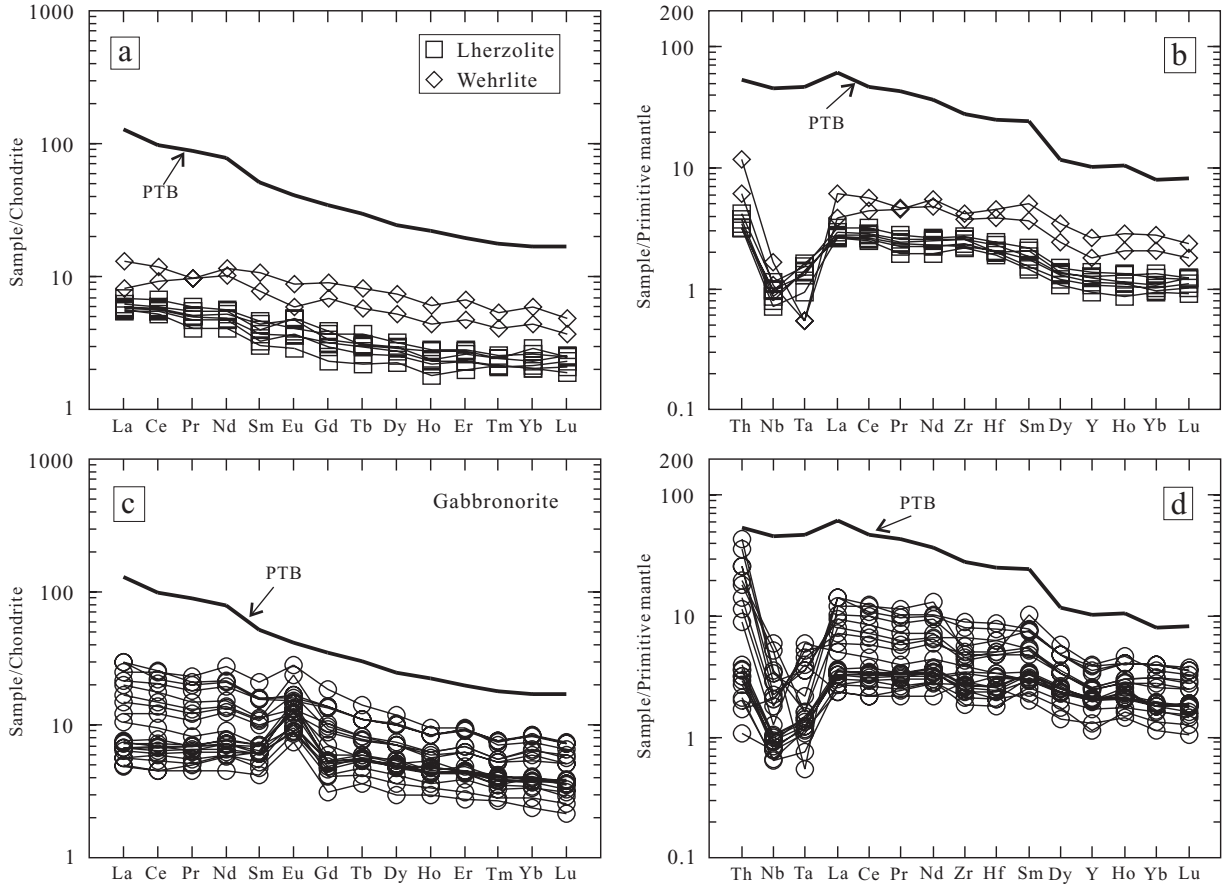

FIG. 6. Chondrite-normalized REE and mantle-normalized immobile trace element patterns of whole-rock samples from the Huangshandong intrusion. The chondrite values are from Anders and Grevesse (1989). The primitive mantle values are from Sun and McDonough (1989). Data for Permian Tarim basalts (PTB) are from Zhou et al. (2009) and Yuan et al. (2012). Data for global volcanic arc basalts (VAB) are from a public database (http://www. petdb.org).

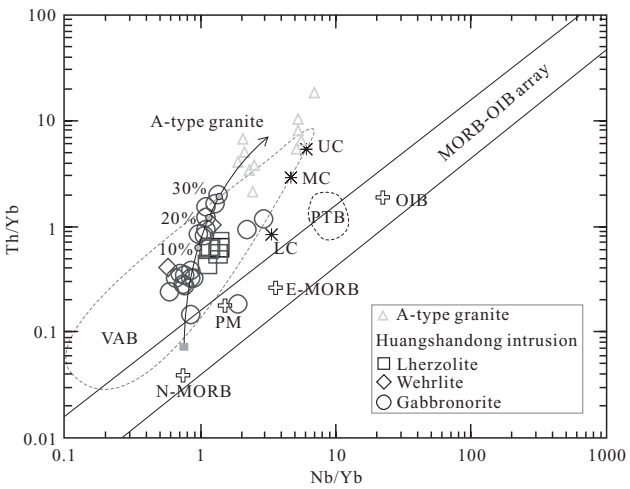

FIG. 7. Plot of whole-rock Th/Yb vs. Nb/Yb for the Huangshandong mafic-ultramafic intrusion. The values of the upper, middle, and lower crusts (UC, MC, LC) are from Rudnick and Gao (2003). The values of the primitive mantle (PM) are from McDonough and Sun (1995). Data for OIB, N-MORB, and E-MORB are from Sun and McDonough (1989). Data for Permian Tarim basalts (PTB) are from Zhou et al. (2009) and Yuan et al. (2012). Data for global volcanic arc basalts (VAB) are from a public database (http://www. petdb.org). Data for A-type granites are from Wang et al. (2009).

In the plot of ε_{Hf} versus ε_{Nd} (Fig. 11c), the Huangshandong samples plot far away from the field of Permian basalts and coeval mafic-ultramafic dikes in the Tarim craton, close to the field of global volcanic arc basalts, and entirely within the MORB field. In the plot of $(^{87}Sr/^{86}Sr)_i$ versus $(^{206}Pb/^{204}Pb)_i$, the Huangshandong samples plot within the MORB field, overlapping with the field of global volcanic arc basalts, and away from the fields of Permian basalts and coeval mafic-ultramafic dikes in the Tarim craton.

Modeling and Discussion

Controls on PGE tenors

Weak to good correlations between most PGE and S contents in whole-rock samples from the Huangshandong intrusion (see Fig. 8), coupled with higher PGE abundances in the sulfide-mineralized samples than the sulfide-poor samples (see Fig. 9), indicate that the distributions of PGE in the intrusion were primarily controlled by magmatic sulfides. Lack of correlations between S and some chalcophile elements, such as Cu and Pt in the Huangshandong intrusion, may be related to compositional variations of sulfide liquids or redistribution of these elements at subsolidus state on cooling or during post-magmatic hydrothermal alteration. The primary controls on

TABLE 1. Concentrations of S, Ni, Cu, and PGE in the Huangshandong Mafic-Ultramafic Intrusion

Sample no.	Rock type	Sulfide mineralization	S	Ni	Cu	Os	Ir	Ru	Rh	Pt	Pd
HD10/1	Gabbronorite	Not visible	na	57	56	0.07	0.06	0.71	0.06	0.66	0.63
HD7/1	Wehrlite	Not visible	na	266	80	0.07	0.06	0.71	0.06	0.82	0.7
HSD-39	Gabbro	Weakly disseminated	na	870	511	0.14	0.08	0.32	0.07	1.74	1.78
YKS-18	Gabbro	Weakly disseminated	na	2,165	1,366	0.19	0.1	0.29	0.14	3.64	2.38
YKS-12	Gabbronorite	Weakly disseminated	na	2,079	1,913	0.13	0.1	0.38	0.18	13.1	7.63
YKS-14	Gabbronorite	Weakly disseminated	na	5,014	2,848	0.39	0.33	0.39	0.54	19.4	11.3
HDK3-3	Gabbronorite	Disseminated sulfides	4.65	5,113	2,359	7.3	0.76	4.49	0.58	7.62	5.72
HDK4-6	Gabbronorite	Disseminated sulfides	10.68	15,410	11,120	4.28	1.74	9.22	2.29	10.6	12.6
HDK1-6	Gabbronorite	Net-textured sulfides	16.28	26,980	14,330	1.39	0.88	7.34	1.74	19.8	15.1
HDK2-4	Lherzolite	Semimassive sulfides	25.21	66,640	4,683	27.1	14.4	41.2	7.83	65	89.3
HDK1-1	Lherzolite	Massive sulfides	30.97	53,590	1,445	8.01	6.41	11.1	6.04	13.8	27

Notes: na = not analyzed, S in wt%, Ni and Cu in ppm, PGE in ppb

the concentrations of PGE in sulfide liquids include the initial contents of these metals in the parental magma, the R factor (sulfide/magma, mass ratio) during sulfide segregation, and fractional crystallization of monosulfide solid solution (mss) from sulfide liquid. Available experimental data indicate that all PGE behave similarly during sulfide segregation and that IPGE (Ir, Os, Ru, Rh) are compatible in mss, whereas PPGE (Pt, Pd) are incompatible in mss (see summary in Naldrett, 2011). In the Huangshandong deposit Ir and Pd are best correlated with S in each of these two different PGE groups (Fig. 8). Hence, these two elements are the best choices for modeling the primary controls on PGE fractionation in the

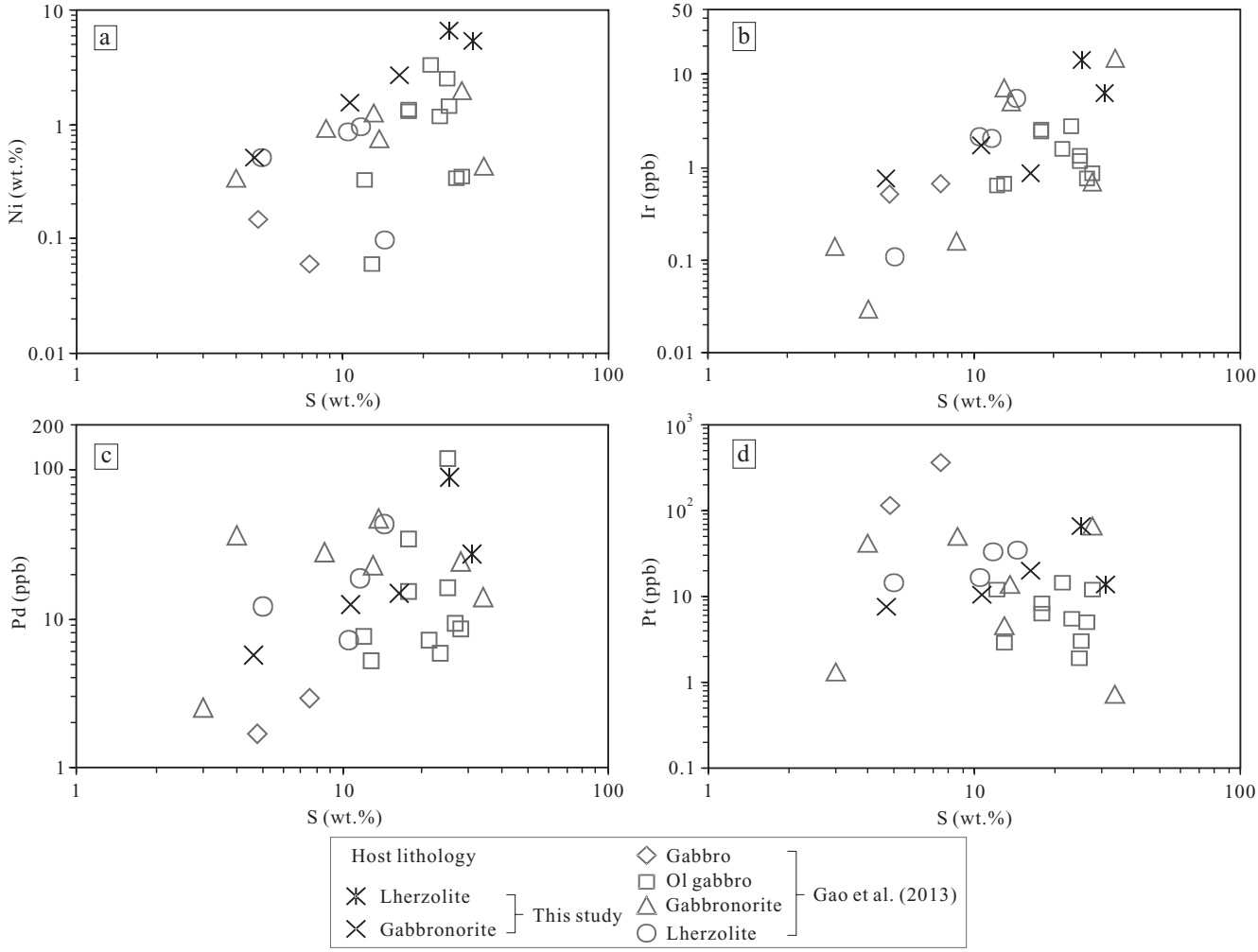

FIG. 8. Plots of Ni, Ir, Pd, and Pt vs. S in sulfide-bearing samples from the Huangshandong magmatic sulfide deposit. Ol = olivine.

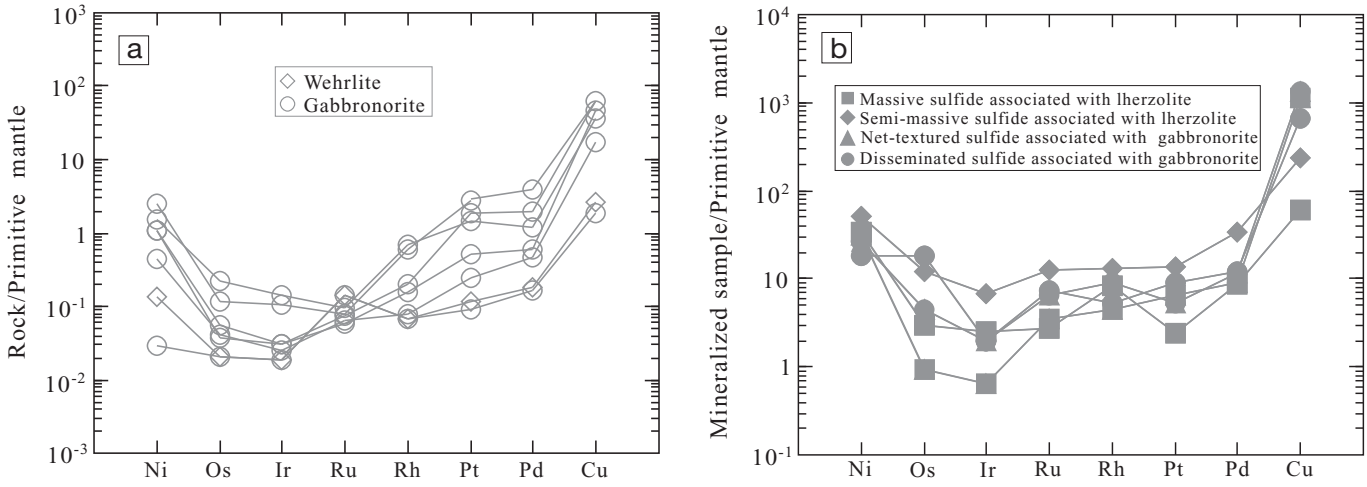

FIG. 9. Primitive mantle-normalized PGE patterns of sulfide-poor (a) and sulfide-bearing (b) samples from the Huangshandong mafic-ultramafic intrusion. The primitive mantle values are from Barnes and Maier (1999).

Huangshandong magmatic system. The results of modeling are shown in Figure 12. In the calculations the sulfide/magma partition coefficients for both Ir and Pd were assumed to be 10^5; the mss/liquid partition coefficients for Ir and Pd were assumed to be 3.5 and 0.1, respectively. The assumed partition coefficients are within the ranges of experimental results (see summary in Naldrett, 2011). The modeling results indicate that the Ir and Pd tenors (i.e., recalculated 100% sulfide) of disseminated sulfide ores can be explained by a parental magma containing ~0.01 ppb Ir and ~0.1 ppb Pd initially and R factors from ~500 to ~1,600, and that the two massive sulfide ores can be explained by the mixtures of mss and coexisting liquid. The estimated initial Ir and Pd contents in the Huangshandong magma are about two orders of magnitude lower than that of PGE-undepleted basalts from Siberia (Lightfoot and Keays, 2005) and Emeishan (Li et al., 2012b). There are at least three possible explanations for PGE depletions in the parental magma of the Huangshandong deposit: (1) a PGE-depleted source mantle, (2) sulfide retention in the mantle due to low degree of partial melting, and (3) previous sulfide segregation in the staging chamber or during magma ascent. At present there is no information about PGE abundances in the source mantle in this region, which makes it difficult to evaluate the different possibilities properly.

TABLE 2. Hf Isotopes of Zircon from the Huangshandong Mafic-Ultramafic Intrusion

Sample no.	$^{176}Yb/^{177}Hf$	2σ	$^{176}Lu/^{177}Hf$	2σ	$^{176}Hf/^{177}Hf$	2σ	$(^{176}Hf/^{177}Hf)_i$	$\varepsilon_{Hf}(t)$
HD01	0.044042	0.000236	0.001799	0.000009	0.283051	0.000013	0.283042	15.6
HD02	0.031636	0.000045	0.001362	0.000002	0.283073	0.000007	0.283066	16.4
HD03	0.025945	0.000065	0.001121	0.000002	0.283008	0.000007	0.283002	14.2
HD04	0.029814	0.000304	0.001248	0.000012	0.283033	0.000007	0.283027	15.0
HD05	0.031872	0.000183	0.001351	0.000008	0.283026	0.000011	0.283019	14.8
HD06	0.044980	0.000103	0.001896	0.000004	0.283021	0.000008	0.283011	14.5
HD07	0.023698	0.000114	0.000995	0.000004	0.283038	0.000008	0.283033	15.3
HD08	0.031377	0.000091	0.001341	0.000004	0.283037	0.000007	0.283030	15.2
HD09	0.038425	0.000067	0.001654	0.000003	0.283037	0.00001	0.283028	15.1
HD10	0.024254	0.000040	0.001050	0.000002	0.283014	0.000012	0.283008	14.4
HD11	0.019305	0.000333	0.000860	0.000014	0.283022	0.000007	0.283017	14.7
HD12	0.024107	0.000169	0.001017	0.000007	0.283063	0.000007	0.283057	16.1
HD13	0.021797	0.000035	0.001004	0.000002	0.283028	0.00001	0.283023	14.9
HD14	0.050167	0.000141	0.002129	0.000005	0.283075	0.000007	0.283064	16.4
HD15	0.038228	0.000136	0.001572	0.000006	0.283070	0.000009	0.283062	16.3
HD16	0.032124	0.000234	0.001391	0.000010	0.283024	0.000008	0.283017	14.7
HD17	0.025215	0.000033	0.001050	0.000001	0.283021	0.000008	0.283016	14.6
HD18	0.018502	0.000218	0.000817	0.000009	0.283016	0.000009	0.283012	14.5
HD19	0.013483	0.000078	0.000602	0.000003	0.283016	0.000007	0.283013	14.6
HD20	0.031484	0.000035	0.001367	0.000002	0.283037	0.000008	0.28303	15.2
HD21	0.046333	0.000185	0.002007	0.000008	0.283014	0.000007	0.283004	14.2
HD22	0.020573	0.000023	0.000970	0.000001	0.283033	0.000010	0.283028	15.1
HD23	0.035730	0.000158	0.001570	0.000007	0.283066	0.000012	0.283058	16.1
HD24	0.030781	0.000261	0.001356	0.000011	0.283077	0.000008	0.283070	16.6
HD25	0.028010	0.000380	0.001214	0.000014	0.283013	0.000007	0.283007	14.3
HD26	0.046331	0.000079	0.002042	0.000003	0.283064	0.000012	0.283054	16.0

Notes: ε_{Hf} calculated using the method of Blichert and Albarede (1997), ^{176}Lu decay constant $\lambda = 1.865 \times 10^{-11}$ y^{-1} (Soderlund et al., 2004), $t = 274$ Ma

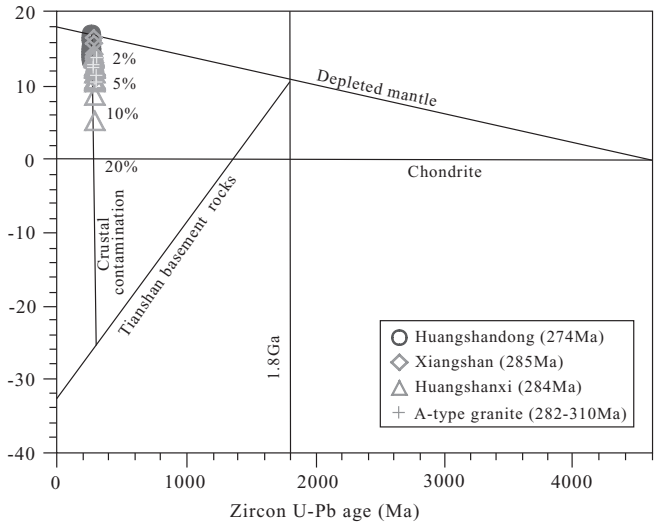

FIG. 10. Plot of ε_{Hf} vs. U-Pb age of zircon from the Huangshandong mafic-ultramafic intrusion. The age of the Tianshan basement is from Hu et al. (2000). The concentration of Hf in the N-type MORB from Sun and McDonough (1989) is used to represent the composition of depleted mantle-derived magma. The evolution of Hf isotopes in the Tianshan basement is calculated using the parameters for the upper crust from Amelin et al. (1999). The Hf isotope data for the Xiangshan and Huangshanxi intrusions and the A-type granites in the region are from Su et al. (2011) and Tang et al. (2008), respectively.

Parental magma composition and timing of sulfide segregation

We have used the method of Li and Ripley (2010) to calculate the composition of parental magma for the Huangshandong ultramafic rocks. The method of Li and Ripley (2010) can only be applied to olivine cumulates. In addition to olivine, some ultramafic rock samples from the Huangshandong intrusion also contain cumulus plagioclase (see Fig. 4b). Since plagioclase contains almost no MgO and higher Al_2O_3 than coexisting magma, the abundances of Al_2O_3 and MgO together can be used to filter out the samples that contain cumulus plagioclase. At a given MgO content, the higher the Al_2O_3 content the more likely cumulus plagioclase is present in the sample. After an evaluation based on this data, we selected a lherzolite sample with the lowest Al_2O_3 content (sample XH04-17) from the Huangshandong intrusion to estimate the composition of parental magma for its ultramafic rocks. The anhydrous composition of this sample, the composition of the most primitive olivine in the intrusion (Fo = 82.5 mol %), and an olivine-liquid Fe-Mg exchange coefficient [$K_d = (FeO/MgO)^{Ol}/(FeO/MgO)^{Liq}$] of 0.3 from Roeder and Emslie (1970) were used in the calculations. The estimated MgO and FeO contents in the parental magma are 7.4 and 8.4 wt %, respectively. The concentrations of other major oxides in the magma are given in Table A2. A simulation using the MELTS program of Ghiorso and Sack (1995) shows that olivine and plagioclase will start to crystallize together from this magma at 1,250°C under the conditions of 1 kb total pressure and QFM-1 oxidation state. The change in olivine Fo content during fractional crystallization is included in the results from the MELTS simulation. The change in olivine Ni content during olivine fractional crystallization with or

TABLE 3. Whole-Rock Rb-Sr-Sm-Nd-Pb Concentrations and Isotopes of the Huangshandong Mafic-Ultramafic Intrusion

Sample no.no.	Rock type	Sm (ppm)	Nd (ppm)	$^{143}Nd/^{144}Nd$	ε_{Nd}	Rb (ppm)	Sr (ppm)	$^{87}Sr/^{86}Sr$	$(^{87}Sr/^{86}Sr)_i$	$(^{206}Pb/^{204}Pb)_i$	$(^{207}Pb/^{204}Pb)_i$	$(^{208}Pb/^{204}Pb)_i$
XH04-12	Lherzolite	0.62	2.79	0.512952	8.29	2.61	153	0.703326	0.703326			
XH04-13	Lherzolite	0.89	3.33	0.512961	7.53	3.68	125	0.703455	0.703455			
XH04-14	Lherzolite	0.76	3.23	0.512965	8.29	5.47	79.1	0.703867	0.703088			
HD12/1	Wehrlite	2.04	6.88	0.512919	7.8	1.13	243	0.703179	0.703200	17.698	15.397	37.138
HD10/1	Gabbronorite	2.23	9.08	0.512889	6.6	9.29	541	0.703726	0.703500	17.951	15.477	37.348
HD11/1	Gabbronorite	3.03	12.5	0.512889	6.7	15.4	482	0.704145	0.703800	17.907	15.458	37.197
XH04-1	Gabbro	1.37	4.7	0.512982	7.46	2.65	435	0.703376	0.703307	17.942	15.477	37.541
XH04-3	Gabbro	1.38	4.56	0.512987	7.32	2.63	428	0.703345	0.703275			
XH04-6	Gabbro	1.04	3.61	0.51299	7.66	0.74	426	0.703415	0.703415			
XH04-8	Gabbro	1.34	4.22	0.513003	7.28	1.47	377	0.703223	0.703223			

Notes: $(^{87}Sr/^{86}Sr)_i$ and ε_{Nd} were calculated relative to present-day chondrite values $^{143}Nd/^{144}Nd = 0.512638$, $^{147}Sm/^{144}Nd = 0.1967$, $^{87}Sr/^{86}Sr = 0.7045$, $^{87}Rb/^{86}Sr = 0.0816$, and λ (^{87}Rb) = 1.42×10^{-11} y^{-1}, λ (^{147}Sm) = 6.54×10^{-12} y^{-1}, $^{87}Sr/^{86}Sr = 0.7045$ and $^{87}Rb/^{86}Sr = 0.0816$; λ (^{87}Rb) = 1.42×10^{-11} y^{-1}, λ (^{147}Sm) = 6.54×10^{-12} y^{-1}; the initial Pb isotope ratios were calculated using λ (^{206}Pb) = 1.55125×10^{-10} y^{-1}, λ (^{207}Pb) = 9.8485×10^{-10} y^{-1}, λ (^{208}Pb) = 0.49475×10^{-10} y^{-1}, t = 274 Ma

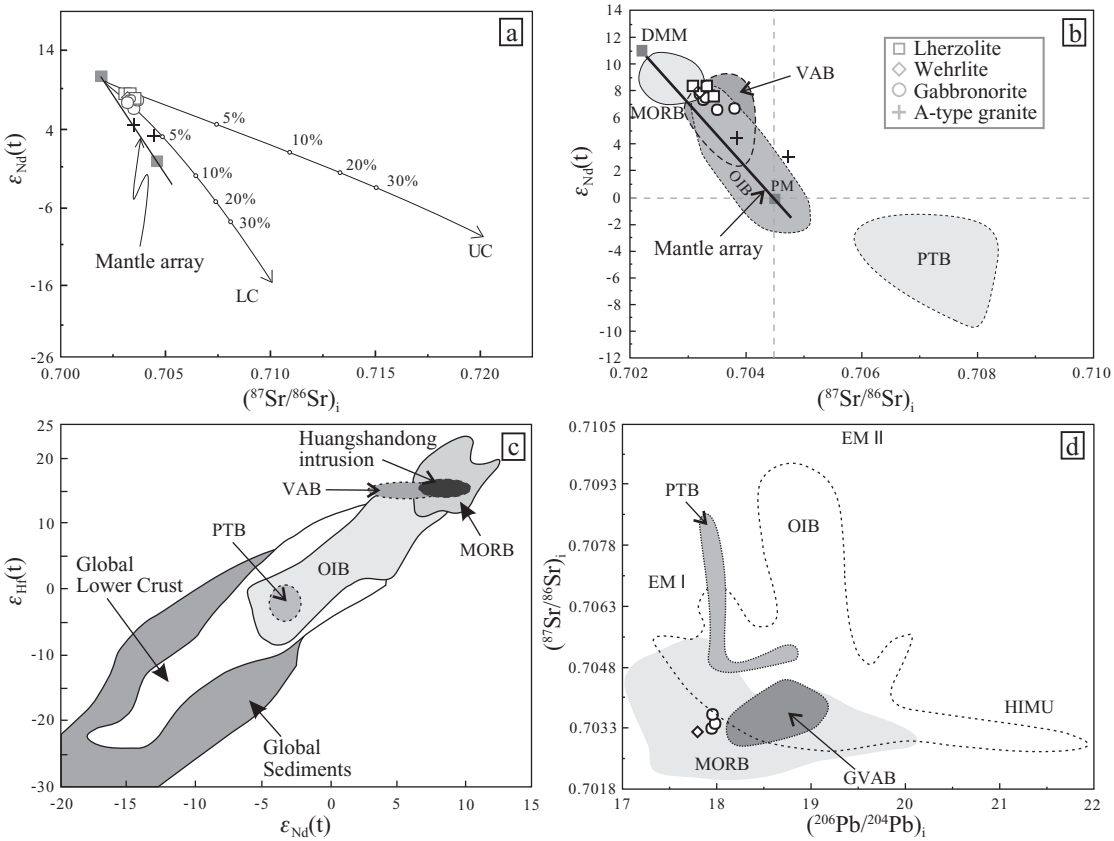

FIG. 11. Plots of Sr-Nd-Hf-Pb isotope systematics for the Huangshandong mafic-ultramafic intrusion. Data for a depleted mantle-derived melt (DMM) and the lower and upper crusts (LC, UC) are from Zindler and Hart (1986) and Rudnick and Gao (2003), respectively. The field of global sediments is from Dobosi et al. (2003). Data for global volcanic arc basalts (VAB) are from a public database (http://www.petdb.org). Data for Permian Tarim basalts (PTB) are from Zhou et al. (2009) and Yuan et al. (2012). Data for Permian A-type granites in East Tianshan are from Wang et al. (2009).

without sulfide segregation can be simulated using the simple Rayleigh fractionation equation. We have used an assumed sulfide/magma D^{Ni} of 500 and an assumed plagioclase/magma D^{Ni} of 0.1, and the olivine/magma D^{Ni} value estimated using the equation of Li and Ripley (2010) to model these processes. The assumed sulfide/magma D^{Ni} value is within the range of experimental results for basaltic systems (see summary in Naldrett, 2011). Our modeling results indicate that fractional crystallization of olivine plus plagioclase without sulfide segregation cannot explain the observed Fo-Ni relationship of olivine in the ultramafic rocks of the Huangshandong intrusion (Fig. 5). Sulfide segregation from the magma during crystallization is required to explain the compositions of olivine in the ultramafic rocks (Fig. 5), implying that sulfide segregation took place as soon as olivine started to crystallize from the Huangshandong magma.

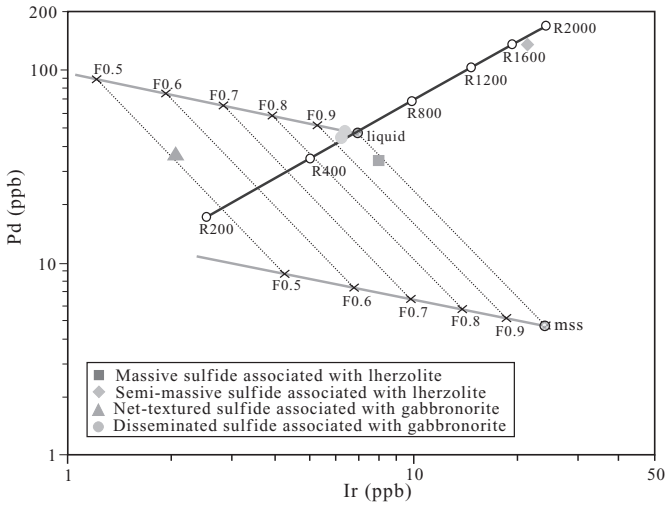

FIG. 12. Modeling of PGE compositional variations as the results of sulfide segregation from magma with variable R factors, using the equation of Campbell and Naldrett (1979) and fractional crystallization of monosulfide solid solution (mss) from sulfide liquid for the Huangshandong magmatic Ni-Cu sulfide deposit. See text for explanation.

Crustal contamination and sulfide saturation

Our Hf-Sr-Nd isotopes indicate that the primary magma of the Huangshandong intrusion was derived from a depleted mantle and that the parental magma of the intrusion may have experienced <2% contamination if the contaminant was the average upper crust (Figs. 10, 11a-b). However, the degree of contamination could be much higher if the contaminant was similar to Permian A-type granites in the region, which have isotopic compositions similar to that of the Huangshangdong intrusion (Figs. 10, 11a-b). Using the average composition of

the A-type granites to represent the contaminant, mixing calculations indicate that the Huangshandong magma may have experienced up to 30% crustal contamination (Fig. 7). Based on these observations, we propose that the parental magma of the Huangshandong intrusion formed by mixing between a depleted mantle-derived magma and a granitic melt formed by magma underplating in a juvenile arc crust. A similar model has been proposed previously by other researchers for several coeval sulfide ore-bearing intrusions, including the Tianyu and Huangshanxi intrusions (Tang et al., 2011; Zhang, M., et al., 2011). No A-type granites are found in the immediate country rocks of the Huangshandong intrusion, indicating that the magma mixing event took place at depth. The hybrid magma may have become sulfide saturated mainly due to decreasing temperature (Li and Naldrett, 1993; Li and Ripley, 2009). If all immiscible sulfide liquids were left behind, the magma would become sulfide unsaturated during magma ascent because of negative effect of total pressure on sulfur content at sulfide saturation in mafic magma (e.g., Mavrogenes and O'Neill, 1999). Given the facts of elevated γ_{Os} values (~100; Mao et al., 2003), mantle-like $\delta^{34}S$ values (–0.8 to +2.8‰; Wang et al., 1987) and extremely low PGE tenors in the Huangshandong sulfide ores, together with the evidence of sulfide segregation during olivine crystallization described above, we suggest that the sulfide ores in the Huangshandong intrusion formed by a second event of sulfide saturation due to fractional crystallization plus addition of external sulfides with mantle-like $\delta^{34}S$ values from juvenile arc crust.

Conclusions

Several important conclusions from this study are summarized below:

1. The parental magma of the Huangshandong Ni-Cu sulfide deposit was a PGE-depleted, evolved basaltic magma containing <7 wt % MgO.
2. Hf-Sr-Nd isotopes and trace elements indicate that mixing between a depleted mantle-derived magma and a partial melt of a juvenile arc crust took place at depth. PGE depletion in the magma may have resulted from sulfide segregation induced by magma mixing.
3. Olivine data indicate that the second event of sulfide segregation took place during olivine crystallization.
4. Fractional crystallization and addition of external sulfides with mantle-like S isotope compositions from juvenile arc crust appear to have played a critical role in triggering the second event of sulfide segregation to form the Huangshandong deposit.

Acknowledgments

This study was financially supported by the National Science Foundation of China (41172090, 41072056), China Geological Survey (1212011085061, 1212011121092), and Chang'an University (CHD2011TD007, CHD2012JC004, CHD2011SY014). We sincerely thank Jinzhu San, Junhui Xie, and Fu Du for logistic support and assistance in fieldwork, and Xiaoming Liu and Hong Zhang for guidance in zircon Hf isotope analysis. Critical comments from two anonymous reviewers and editorial inputs from guest editors Christina Wang and Steve Barnes are greatly appreciated.

References

Amelin, Y., Lee, D.-C., Halliday, A.N., and Pidgeon, R.T., 1999, Nature of the earth's earliest crust from hafnium isotopes in single detrital zircons: Nature, v. 399, p. 252–255.

Anders, E., and Grevesse N., 1989, Abundances of the elements: Meteoritic and solar: Geochimica et Cosmochimica Acta, v. 53, p. 197–214.

Barnes, S-J., and Maier, W.D., 1999, The fractionation of Ni, Cu, and the noble metals in silicate and sulphide liquids: Geological Association of Canada Short Course Notes, v. 13, p. 69–106.

Blichert, T.J., and Albarede, F., 1997, The Lu-Hf geochemistry of the chondrites and the evolution of the mantle-crust system: Earth and Planetary Science Letters, v. 148, p. 243–258.

Branquet, Y., Gumiaux, C., Sizaret, S., Barbanson, L., Wang, B., Cluzel, D., Li, G., and De Launay, A., 2012, Synkinematic mafic/ultramafic sheeted intrusions: Emplacement mechanism and strain restoration of the Permian Huangshan Ni-Cu ore belt (Eastern Tianshan, NW China): Journal of Asian Earth Sciences, v. 56, p. 240–257.

Campbell, I.H., and Naldrett, A.J., 1979, The influence of silicate:sulfide ratios on the geochemistry of magmatic sulfides: Economic Geology, v. 74, p. 1503–1505.

Dobosi, G., Downes, H., Embey-Isztin, A., and Jenner, G.A., 2003, Origin of megacrysts and pyroxenite xenoliths from the Pliocene alkali basalts of the Pannonian basin (Hungary): Neues Jahrbuch Fur Mineralogie-Abhandlungen, v. 178, p. 217–237.

Gao, J.-F., Zhou, M.-F., Lightfoot, P.C., Wang, C.Y., Qi, L., and Sun, M., 2013, Sulfide-saturation and magma emplacement in the formation of the Permian Huangshandong Ni-Cu sulfide deposit, Xinjiang, northwestern China: Economic Geology, v. 108, p. 1833–1848.

Ghiorso, M.S., and Sack, R.O., 1995, Chemical mass transfer in magmatic processes. IV. A revised and internally consistent thermodynamic model for the interpolation and extrapolation of liquid-solid equilibria in magmatic systems at elevated temperatures and pressures: Contributions to Mineralogy and Petrology, v. 119, p. 197–212.

Han, B.-F., Ji, J.-Q., Song, B., Chen, L.-H., and Li, Z.-H., 2004, SHRIMP zircon U-Pb ages of Karatongke No. 1 and Huangshandong Cu-Ni-bearing mafic-ultramafic complexes, North Xinjiang, and geological implications: Chinese Science Bulletin, v. 49, p. 2424–2429.

Hu, A.Q., Jahn, B.-M., Zhang, G., Chen, Y., and Zhang, Q., 2000, Crustal evolution and Phanerozoic crustal growth in northern Xinjiang: Nd isotopic evidence. Pt I. Isotopic characterization of basement rocks: Tectonophysics, v. 328, p. 15–51.

Jahn, B.-M., 2004, The Central Asia orogenic belt and growth of the continental crust in the Phanerozoic: Geological Society of London Special Publication 226, p. 73–100.

Jiang, C.Y., Cheng, S.L., Ye, S.F., Xia, M.Z, Jiang, H.B., and Dai, Y.C., 2006, Lithogeochemistry and petrogenesis of Zhongposhanbei mafic rock body at Beishan region, Xinjiang: Acta Petrologica Sinica, v. 22, p. 115–126 (in Chinese).

Li, C., and Naldrett, A.J., 1993, Sulfide capacity of magma: A quantitative model and its application to the formation of sulfide ores at Sudbury, Ontario: Economic Geology, v. 88, p. 1253–1260.

Li, C., and Ripley, E.M., 2009, Sulfur contents at sulfide-liquid or anhydrite saturation in silicate melts: Empirical equations and example applications: Economic Geology, v. 104, p. 405–412.

——2010, The relative effects of composition and temperature on olivine-liquid Ni partitioning: Statistical deconvolution and implications for petrologic modeling: Chemical Geology, v. 275, p. 99–104.

Li, C., Zhang, M.J., Fu, P.E., Qian, Z.Z., Hu, P.Q., and Ripley, E.M., 2012a, The Kalatongke magmatic Ni-Cu deposit in the Central Asian orogenic belt, NW China: Product of slab window magmatism?: Mineralium Deposita, v. 47, p. 51–67.

Li, C., Tao, Y., Qi, L., and Ripley, E.M., 2012b, Controls on PGE fractionation in the Emeishan picrites and basalts: Constraints from integrated lithophile-siderophile elements and Sr-Nd isotopes: Geochimica et Cosmochimica Acta, v. 90, p. 12–32.

Li, D., Bao, X., and Zhang, B., 1989, Geology, geophysics and geochemistry of the Huangshan Cu-Ni metallogenic belt and exploration implications: Report to the Office of the National 305 Project of China, 418 p. (in Chinese).

Li, H.Q., Chen, F.W., Mei, Y.P., Wu, H., Cheng, S.L., Yang, J.Q., and Dai, Y.C., 2006, Dating of the No.1 intrusion of Pobei basic-ultrabasic rocks belt, Xinjiang, and its geological significance: Mineral Deposits, v. 25, p. 463–469 (in Chinese).

Lightfoot, P.C., and Keays, R.R., 2005, Siderophile and chalcophile metal variations in flood basalts from the Siberian trap, Noril'sk region: Implications for the origin of the Ni-Cu-PGE sulfide ores: Economic Geology, v. 100, p. 439–462.

McDonough, W.W., and Sun, S.-S., 1995, The composition of the Earth: Chemical Geology, v. 120, p. 223–253.

Mao, J., Yang, J., Qu, W., Du, A., Wang, Z., and Han, C., 2003, Re-Os age of Cu-Ni ores from the Huangshandong Cu-Ni sulfide deposit in the East Tianshan Mountains and its implication for geodynamic processes: Acta Geologica Sinica, v. 77, p. 220–226 (in Chinese with English abs.).

Mavrogenes, J.A., and O'Neill, H.S.C., 1999, The relative effects of pressure, temperature and oxygen fugacity on the solubility of sulfide in mafic magmas: Geochimica et Cosmochimica Acta, v. 63, p. 1173–1180.

Naldrett, A.J., 2011, Fundamentals of magmatic sulfide deposits: Reviews in Economic Geology, v. 17, p. 1–50.

Qin, K.-Z., Su, B.-X., Sakyi, P.A., Tang, D.-M., Li, X.-H., Sun, H., Xiao, Q.-H., and Liu, P.-P., 2011, SIMS zircon U-Pb geochronology and Sr-Nd isotopes of Ni-Cu-bearing mafic-ultramafic intrusions in eastern Tianshan and Beishan in correlation with flood basalts in Tarim basin (NW China): Constraints on a ca. 280 Ma mantle plume: American Journal of Science, v. 311, p. 237–260.

Roeder, P.L., and Emslie, R.F., 1970, Olivine-liquid equilibrium: Contributions to Mineralogy and Petrology, v. 29, p. 275–289.

Rudnick, R.L., and Gao, S., 2003, Composition of the continental crust: Treatise on Geochemistry, v. 3, p. 1–64.

San, J.-Z., Qin, K.-Z., Tang, D.-M., Su, B.-X., Sun, H., Xiao, Q.-H., Liu, P.-P., and Cao, M.-J., 2010, Precise zircon U-Pb ages of Tulargen large Cu-Ni ore-bearing mafic-ultramafic complex and their geological implications: Acta Petrologica Sinica, v. 26, p. 3027–3035 (in Chinese with English abs.).

Shu, L., Wang, B., Zhu, W., Guo, Z., Charvet, J., and Zhang, Y., 2011, Timing of initiation of extension in the Tianshan, based on structural, geochemical and geochronological analyses of bimodal volcanism and olistostrome in the Bogda Shan (NW China): International Journal of Earth Sciences, v. 100, p. 1647–1663.

Soderlund, U., Patchett, J.P., Vervoort, J.D., and Isachsen, C.E., 2004, The Lu-176 decay constant determined by Lu-Hf and U-Pb isotope systematics of Precambrian mafic intrusions: Earth and Planetary Science Letters, v. 219, p. 311–324.

Song, X.-Y., Xie, W., Deng, Y.-F., Crawford, A.J., Zheng, W.-Q., Zhou, G.-F., Deng, G., Cheng, S.-L., and Li, J., 2011, Slab break-off and the formation of Permian mafic-ultramafic intrusions in southern margin of Central Asian orogenic belt, Xinjiang, NW China: Lithos, v. 127, p. 128–143.

Su, B.-X., Qin, K.-Z., Patrick Asamoah Sakyi, Li, X.-H., Yang, Y.-H., Sun, H., Tang, D.-M., Liu, P.-P., Xiao, Q.-H., and Malaviarachchi, S.P.K., 2011, U-Pb ages and Hf-O isotopes of zircons from Late Paleozoic mafic-ultramafic units in the southern Central Asian orogenic belt: Tectonic implications and evidence for an Early-Permian mantle plume: Gondwana Research, v. 20, p. 516–531.

Su, B.-X., Qin, K.Z., Sakyi, P.A., Malaviarachchi, S.P.K., Liu, P.-P., Tang, D.-M., Xiao, Q.-H., Sun, H., Ma, Y.-G., and Mao, Q., 2012, Occurrence of an Alaskan-type complex in the Middle Tianshan Massif, Central Asian orogenic belt: Inferences from petrological and mineralogical studies: International Geology Review, v. 54, p. 249–269.

Sun, S.-S., and McDonough, W.F., 1989, Chemical and isotopic systematics in ocean basalt: Implication for mantle composition and processes: Geological Society of London Special Publication 42, p. 313–345.

Sun, T., Qian, Z.Z., Tang, Z.L., Jiang, C.Y., He, K., Sun, Y.L., Wang, J.Z., and Xia, M.Z., 2010, Zircon U-Pb chronology, platinum group element geochemistry characteristics of Hulu Cu-Ni deposit, East Xinjiang, and its geological significance: Acta Petrologica Sinica, v. 26, p. 3339–3349 (in Chinese with English abs.).

Sun, Y., and Sun, M., 2005, Nickel sulfide fire assay improved for pre-concentration of platinum group elements in geological samples: A practical means of ultra-trace analysis combined with inductively coupled plasma-mass spectrometry: The Analyst, v. 130, p. 664–669.

Sun, Y.L., Chu, Z., Sun, M., and Xia, X., 2009, An improved Fe-Ni fire assay method for determination of Re, platinum group elements, and Os isotopic ratios by inductively coupled plasma- and negative thermal ionization-mass spectrometry: Applied Spectroscopy, v. 63, p. 1232–1237.

Tang, D.-M., Qin, K.-Z., Li, C., Qi, L., Su, B.-X., and Qu, W.-J., 2011, Zircon dating, Hf-Sr-Nd-Os isotopes and PGE geochemistry of the Tianyu sulfide-bearing mafic-ultramafic intrusion in the Central Asian orogenic belt, NW China: Lithos, v. 126, p. 84–98.

Tang, H.-F., Zhao, Z.-Q., Huang, R.-S., Han, Y.-J., and Su, Y.-P., 2008, Primary Hf isotopic study on zircons from the A-type granites in eastern Junggar of Xinjiang, NW China: Acta Mineraligica Sinica, v. 28, p. 335–342 (in Chinese).

Tian, W., Campbell, I.H., Allen, C.M., Guan, P., Pan, W., Chen, M., Yu, H., and Zhu, W., 2010, The Tarim picrite-basalt-rhyolite suite, a Permian flood basalt from northwest China with contrasting rhyolites produced by fractional crystallization and anatexis: Contributions to Mineralogy and Petrology, v. 160, p. 407–425.

Wang, B., Faure, M., Shu, L., de Jong, K., Charvet, J., Cluzel, D., Jahn, B.-M., Chen, Y., and Ruffet, G., 2010, Structural and geochronological study of high-pressure metamorphic rocks in the Kekesu section (northwestern China): Implications for the late Paleozoic tectonics of the southern Tianshan: Journal of Geology, v. 118, p. 59–77.

Wang, C.S., Gu, L.X., Zhang, Z.Z., Wu, C.Z., Tang, J.H., and Tang, X.Q., 2009, Petrogenesis and geological implications of the Permian high-K calc-alkaline granites in Harlik Mountains of eastern Tianshan, NW China: Acta Petrologica Sinica, v. 25, p. 1499–1511 (in Chinese with English abs.).

Wang, R., Liu, D., and Yin, D., 1987, The conditions of controlling metallogeny of Cu-Ni sulfide ore deposits and the orientation of finding ore Hami, Xingjiang, China: Minerals and Rocks, v. 7, p. 1–178 (in Chinese).

Wang, Y.W., Wang, J.B., Wang, L.J., and Long, L.L., 2008, Zircon U-Pb age, Sr-Nd isotope geochemistry and geological significances of the Weiya mafic-ultramafic complex, Xinjiang: Acta Petrologica Sinica, v. 24, p. 781–792 (in Chinese with English abs.)

Xiao, Q.H., Qin, K.Z., Tang, D.M., Su, B.X., San, J.Z., Cao, M.J., and Hui, W.D., 2010, Xiangshanxi composite Cu-Ni-Ti-Fe deposite belongs to comagmatic evolution product: Evidences from ore microscopy, zircon U-Pb chronology and petrological geochemistry, Hami, Xinjiang, NW China: Acta Petrologica Sinica, v. 26, p. 503–522 (in Chinese with English abs.).

Xiao, W., Windley, B.F., Hao, J., and Zhai, M., 2003, Accretion leading to collision and the Permian Solonker suture, Inner Mongolia, China: Termination of the Central Asian orogenic belt: Tectonics, v. 22, p. 1069, 20 p., doi:10.1029/2002TC001484.

Xiao, W.-J., Zhang, L.-C., Qin, K.-Z., Sun, S., and Li, J.-L., 2004, Paleozoic accretionary and collisional tectonics of the eastern Tianshan (China): Implications for the continental growth of central Asia: American Journal of Science, v. 304, p. 370–395.

Xiao, W.J., Windley, B.F., Huang, B.C., Han, C.M., Yuan, C., Chen, H.L., Sun, M., Sun, S., and Li, J.L., 2009, End-Permian to mid-Triassic termination of the accretionary processes of the southern Altaids: Implications for the geodynamic evolution, Phanerozoic continental growth, and metallogeny of Central Asia: International Journal of Earth Sciences, v. 98, p. 1189–1217.

Yang, S.-H., and Zhou, M.-F., 2009, Geochemistry of the 430-Ma Jingbulake mafic-ultramafic intrusion in western Xinjiang, NW China: Implications for subduction related magmatism in the South Tianshan orogenic belt: Lithos, v. 113, p. 259–273.

Yuan, C., Sun, M., Wilde, S., Xiao, W., Xu, Y., Long, X., and Zhao, G., 2010, Post-collisional plutons in the Balikun area, East Chinese Tianshan: Evolving magmatism in response to extension and slab break-off: Lithos, v. 119, p. 269–288.

Yuan, F., Zhou, T.F., Zhang, D., Fan, Y., Jowitt. S.J., Keays, R.R., Liu, S., and Fan, Y., 2012, Siderophile and chalcophile metal variations in basalts: Implications for the sulfide saturation history and Ni-Cu-PGE mineralization potential of the Tarim continental flood basalt province, Xinjiang Province, China: Ore Geology Reviews, v. 45, p. 5–15.

Yuan, H.-L., Gao, S., Dai, M.-N., and Liu, X.-M., 2008, Simultaneous determinations of U-Pb age, Hf isotopes and trace element compositions of zircon by excimer laser ablation quadrupole and multiple collectors ICP-MS: Chemical Geology, v. 247, p. 100–117.

Zhang, C.-L., Yang, D.-S., Wang, H.-Y., Yutaka, T., and Ye, H.-M., 2011, Neoproterozoic mafic-ultramafic layered intrusion in Quruqtagh of northeastern Tarim block, NW China: Two phases of mafic igneous activity with different mantle sources: Gondwana Research, v. 19, p. 177–190.

Zhang, M., Li, C., Fu, P., Hu, P., and Ripley, E.M., 2011, The Permian Huangshanxi Cu-Ni deposit in western China: Intrusive-extrusive association, ore genesis, and exploration implications: Mineralium Deposita, v. 46, p. 153–170.

Zhou, D., Liu, Y., Xin, X., Hao, J., Dong, Y., and Ouyang, Z., 2006, Formation of the Permian basalts and implications of geochemical tracing for paleotectonic setting and regional tectonic background in the Turpan-Hami and Santanghu basins, Xinjiang: Science in China (D), v. 49, p. 584–596.

Zhou, M.-F., Lesher, C.M., Yang, Z., Li, J., and Sun, M., 2004, Geochemistry and petrogenesis of 270 Ma Ni-Cu-(PGE) sulfide-bearing mafic intrusions in the Huangshan district, eastern Xinjiang, northwest China: Implications for the tectonic evolution of the Central Asian orogenic belt: Chemical Geology, v. 209, p. 233–257.

Zhou, M.-F., Zhao, J.-H., Jiang, C.-Y., Gao, J.-F., Wang, W., and Yang, S.-H., 2009, OIB-like, heterogeneous mantle sources of Permian basaltic magmatism in the western Tarim basin, NW China: Implications for a possible Permian large igneous province: Lithos, v. 113, p. 583–594.

Zindler, A., and Hart, S.R., 1986, Chemical geodynamics: Annual Review of Earth and Planetary Sciences, v. 14, p. 493–571.

TABLE A1. Compositions of Olivine Crystals Enclosed in Pyroxene and Plagioclase, Huangshandong Intrusion

Sample no.	Rock type	Host	*n*	SiO_2	FeO	MnO	MgO	CaO	NiO	Total	Fo
HSD3	Ol websterite	Pyroxene	6	38.91	18.75	0.28	41.73	na	0.08	99.75	80.02
HSD4	Ol websterite	Pyroxene	5	38.88	18.74	0.27	41.80	na	0.09	99.77	80.06
HSD7	Ol websterite	Pyroxene	23	38.90	18.71	0.27	41.67	na	0.09	99.63	80.03
HSD10	Ol websterite	Pyroxene	7	38.91	18.18	0.27	42.33	0.05	0.12	99.86	80.74
HSD11	Ol websterite	Pyroxene	7	38.86	18.21	0.26	41.83	na	0.09	99.26	80.52
HSD13	Ol websterite	Pyroxene	16	39.07	17.96	0.26	42.49	0.03	0.11	99.92	80.99
XH04-26	Lherzolite	Pyroxene	4	40.28	16.58	0.21	42.18	0.04	0.19	99.46	81.93
XHD08-1	Lherzolite	Pyroxene	4	40.08	16.65	0.23	42.33	0.05	0.18	99.50	81.93
XHD08-5	Lherzolite	Pyroxene	4	40.10	16.88	0.22	42.28	0.04	0.17	99.67	81.70
XH04-20	Lherzolite	Plagioclase	3	39.97	16.93	0.23	42.13	0.02	0.14	99.42	81.63
XHD08-44	Ol gabbro	Plagioclase	2	37.40	25.20	0.32	36.50	0.06	0.03	99.51	72.05
XHD08-49	Ol gabbro	Plagioclase	2	37.25	26.80	0.17	34.65	0.05	0.01	98.92	69.75
XHD08-51	Ol gabbro	Plagioclase	1	36.20	27.00	0.31	36.20	0.04	0.01	99.76	70.50

Notes: na = not analyzed; Ol = olivine

TABLE A2. Whole-Rock Major and Trace Element Compositions of the Huangshandong Intrusion

Sample no.	XH04-12	XH04-13	XH04-14	XH04-15	XH04-16	XH04-17	HD7/1	HD12/1	HD2/1
Rock type			Lherzolite				Wehrlite		Gabbronorite
SiO_2	41.70	41.10	40.60	40.80	40.80	40.90	44.18	39.14	47.58
TiO_2	0.26	0.34	0.31	0.29	0.27	0.21	0.37	0.68	0.67
Al_2O_3	7.49	6.56	7.01	6.65	5.99	5.24	4.80	4.88	19.27
FeO^{total}	14.30	13.40	12.90	13.20	13.90	14.20	10.36	12.22	7.36
MnO	0.15	0.14	0.12	0.14	0.14	0.14	0.14	0.17	0.10
MgO	26.40	27.50	27.10	28.20	28.80	29.60	26.48	27.34	9.50
CaO	3.64	2.92	2.04	2.88	2.65	2.40	5.99	5.95	7.86
Na_2O	1.26	1.64	0.66	1.02	0.96	0.92	0.50	0.37	3.80
K_2O	0.17	0.22	0.29	0.15	0.18	0.15	0.15	0.07	0.25
P_2O_5	0.05	0.06	0.05	0.054	0.056	0.06	0.06	0.06	0.07
LOI	3.5	5.25	8.11	5.4	5.11	4.79	6.31	8.99	3.49
Total	99	99.2	99.2	98.8	98.9	98.6	99.34	99.87	99.95
Sc	20.2	17.8	16.5	17.3	16.6	15.3	38.27	23.01	33.96
V	67	55.7	63.4	60.1	50.9	47.7	101.3	96.63	131.8
Cr	1440	1390	1439	1518	1217	1606	2444	1427	142.5
Ni	543	577	546	553	630	720	266	615	758
Cu	42	52	31	37	73	73	80	107	142
Sr	153	125	79.1	135	121	103	115	243	518
Rb	2.61	3.68	5.47	2.83	3.44	2.65	2.14	1.13	3.04
Y	4.66	5.85	5.36	5.25	4.81	4.07	7.84	11.39	8.3
Zr	24.5	28.4	26.7	26.9	23.2	22.6	39.05	44.51	40.95
Nb	0.53	0.74	0.65	0.63	0.58	0.47	1.09	0.7	0.83
Ba	26.3	35.4	49.5	29.6	23.2	22.6	18.64	13.37	243
Th	0.27	0.33	0.26	0.25	0.30	0.25	0.93	0.49	0.72
U	0.11	0.12	0.11	0.10	0.10	0.09	0.21	0.11	0.23
Pb	1.57	1.42	1.24	1.25	1.26	1.55	1.34	1.81	2.29
Hf	0.57	0.68	0.65	0.56	0.58	0.53	1.08	1.28	0.95
Ta	0.05	0.06	0.05	0.06	0.05	0.04	0.02	0.02	0.22
La	1.69	2.09	1.89	1.82	1.77	1.70	3.95	2.5	3.25
Ce	4.33	5.28	4.75	4.60	4.43	4.20	9.43	7.38	7.70
Pr	0.57	0.72	0.66	0.61	0.60	0.49	1.17	1.15	1.01
Nd	2.79	3.33	3.23	3.09	2.85	2.42	6.00	6.88	5.46
Sm	0.62	0.89	0.76	0.84	0.71	0.58	1.49	2.04	1.39
Eu	0.27	0.29	0.35	0.34	0.26	0.21	0.43	0.64	0.97
Gd	0.76	0.94	0.98	0.84	0.81	0.58	1.74	2.3	1.84
Tb	0.12	0.17	0.14	0.15	0.14	0.10	0.27	0.38	0.27
Dy	0.81	1.00	0.91	0.93	0.87	0.72	1.64	2.34	1.77
Ho	0.16	0.20	0.19	0.17	0.16	0.13	0.31	0.43	0.33
Er	0.48	0.58	0.56	0.54	0.48	0.42	0.98	1.38	1.04
Tm	0.07	0.08	0.08	0.08	0.07	0.07	0.13	0.17	0.13
Yb	0.45	0.54	0.59	0.47	0.42	0.43	0.91	1.23	0.87
Lu	0.08	0.08	0.08	0.08	0.07	0.06	0.12	0.16	0.12

Sample no.	HD3/1	HD3/2	HD10/1	HD10/2	HD11/1	HD11/2	XHD08-41	XHD08-42	XHD08-43
Rock type					Gabbronorite				
SiO_2	46.43	50.26	51.51	51.08	52.92	52.86	48.80	47.90	48.70
TiO_2	0.68	0.71	0.59	0.89	0.82	0.84	0.44	0.40	0.30
Al_2O_3	17.55	20.16	18.94	18.83	17.27	17.24	20.60	19.20	24.90
FeO^T	8.42	5.88	6.22	6.70	6.89	6.74	5.45	6.04	3.26
MnO	0.12	0.09	0.11	0.11	0.12	0.11	0.10	0.10	0.05
MgO	12.34	6.48	6.48	6.58	6.53	6.36	8.26	9.98	5.06
CaO	8.65	11.13	9.79	9.87	8.33	8.57	13.10	12.60	13.70
Na_2O	2.71	3.24	3.36	3.15	3.86	4.20	2.06	1.84	2.36
K_2O	0.14	0.40	0.46	0.45	0.76	0.63	0.13	0.13	0.09
P_2O_5	0.07	0.1	0.08	0.1	0.13	0.14	0.063	0.068	0.042
LOI	3.01	1.53	2.13	2.2	1.82	1.92	0.59	1.45	1.32
Total	100.12	99.98	99.67	99.96	99.45	99.61	99.6	99.7	99.7
Sc	23.1	17.31	27.67	23.5	17.89	29.67	23.8	26.5	16.4
V	94.1	225.4	110.7	159.1	142	147.9	205	237	122
Cr	139.2	211	70.96	78.47	180.7	178.1	528	559	573
Ni	169	14	57	64	11	107	41	53	42
Cu	51	23	56	72	34	52	10	11	9
Sr	412	576	541	532	482	491	430	398	510
Rb	1.68	7.35	9.29	9.7	15.4	12.89	2.39	2.96	1.17
Y	10.4	10.76	10.99	15.43	16.68	14.59	8.61	8.59	5.57
Zr	50.9	44.99	47.84	59.34	85.46	94.2	36.2	35.3	30.1
Nb	1.2	1.34	1.49	1.89	2.24	2.36	0.67	0.60	0.44

TABLE A2. *(Cont.)*

Sample no.	HD3/1	HD3/2	HD10/1	HD10/2	HD11/1	HD11/2	XHD08-41	XHD08-42	XHD08-43
Rock type					Gabbronorite				
Ba	69.69	96.81	120.1	118.9	199.3	190	36.2	35.3	30.1
Th	0.91	1.14	2.06	2.06	2.86	3.46	0.25	0.29	0.16
U	0.52	0.31	0.31	0.35	0.55	0.72	0.10	0.10	0.07
Pb	1.29	1.84	6.37	5.88	4.65	4.91	0.58	1.24	0.623
Hf	1.36	1.35	1.45	1.78	2.24	2.5	0.95	0.88	0.72
Ta	0.19	0.17	0.13	0.13	0.08	0.06	0.05	0.06	0.04
La	3.81	4.62	6.17	6.73	9.17	9.16	2.1	1.97	1.53
Ce	9.81	11.2	14.24	16.54	17.97	20.9	5.15	4.93	3.69
Pr	1.33	1.48	1.83	2.23	2.47	2.6	0.80	0.76	0.56
Nd	7.50	8.16	9.08	11.79	12.5	12.93	3.95	3.78	2.74
Sm	1.96	2.10	2.23	3.06	3.03	3.14	1.18	1.18	0.82
Eu	0.89	1.25	0.98	1.13	1.23	1.18	0.68	0.64	0.55
Gd	2.30	2.40	2.63	3.47	3.60	3.60	1.26	1.20	0.82
Tb	0.36	0.37	0.39	0.53	0.53	0.53	0.27	0.26	0.17
Dy	2.28	2.26	2.28	3.27	3.19	3.23	1.56	1.59	0.96
Ho	0.43	0.41	0.45	0.60	0.60	0.61	0.34	0.35	0.22
Er	1.33	1.33	1.46	1.95	1.93	1.97	0.95	0.93	0.59
Tm	0.17	0.17	0.18	0.25	0.24	0.25	0.13	0.12	0.09
Yb	1.12	1.24	1.38	1.73	1.76	1.76	0.79	0.79	0.50
Lu	0.17	0.17	0.19	0.24	0.24	0.25	0.13	0.13	0.07

Sample no.	XHD08-49	XH04-1	XH04-2	XH04-3	XH04-4	XH04-6	XH04-7	XH04-8	HD4/2	HD4/3	Estimated
Rock type					Gabbronorite						magma*
SiO_2	44.60	49.70	50.60	48.80	49.90	49.60	49.20	48.30	47.29	48.40	51.92
TiO_2	2.95	0.39	0.47	0.40	0.42	0.39	0.38	0.43	3.33	3.58	0.76
Al_2O_3	20.90	19.90	19.40	19.20	20.40	21.50	20.10	18.00	17.83	17.30	18.82
FeO_T	9.02	5.62	6.26	5.71	5.31	4.97	5.08	6.22	11.96	12.35	8.36
MnO	0.10	0.09	0.10	0.09	0.08	0.08	0.08	0.09	0.16	0.18	0.15
MgO	7.78	7.01	7.89	7.92	6.91	6.86	7.31	9.35	4.77	4.96	7.38
CaO	12.00	10.80	10.90	11.20	10.90	11.50	11.20	11.30	8.81	8.70	8.56
Na_2O	1.90	3.49	2.83	2.97	2.96	2.54	2.50	2.43	3.59	3.37	3.32
K_2O	0.11	0.23	0.20	0.24	0.20	0.11	0.17	0.15	0.37	0.39	0.53
P_2O_5	0.039	0.054	0.052	0.048	0.052	0.039	0.045	0.047	0.78	0.13	0.2
LOI	0.22	2.57	1.31	2.38	1.52	2.3	2.69	2.48	1.42	0.73	
Total	99.7	99.8	100	98.9	98.7	99.8	98.8	98.9	100.31	100.09	100
Sc	43.1	24	24.6	23.5	25.2	24.1	7.27	28.2	11.04	30.87	
V	426	245	234	261	282	188	181	238	201.6	195.1	
Cr	12	312	348	293	390	462	506	816	8.95	7.27	
Ni	17.2	57.8	59.1	57.4	61.2	62.3	64.1	95.3	0.13	0.35	
Cu	21.2	22.6	19.7	23.2	19.3	21.9	15.7	21.6	84.09	85.46	
Sr	557	435	473	428	409	426	388	377	632	574	
Rb	1.57	2.65	3.19	2.63	3.65	0.74	0.73	1.47	6.52	6.87	
Y	8.7	8.96	8.53	8.94	8.85	7.32	4.93	9.17	16.85	11.16	
Zr	28.2	28.7	25	28	25.2	19.4	22.5	26.6	53.67	69.46	
Nb	1.35	0.70	0.55	0.64	0.53	0.42	0.51	0.62	3.41	3.9	
Ba	28.3	45.7	43	42	40.7	31.6	36	38.6	121.2	122.7	
Th	0.13	0.31	0.28	0.29	0.26	0.17	0.09	0.24	1.43	1.56	
U	0.05	0.11	0.22	0.11	0.14	0.07	0.08	0.09	0.43	0.38	
Pb	0.49	1.55	1.47	1.54	1.36	1.1	1.81	1.1	2.33	2.33	
Hf	0.90	0.72	0.67	0.74	0.59	0.52	0.59	0.68	1.42	1.77	
Ta	0.15	0.05	0.04	0.05	0.05	0.03	0.04	0.05	0.02	0.06	
La	1.55	2.36	2.31	2.23	2.10	1.76	1.75	2.10	7.77	5.22	
Ce	3.63	6.25	5.64	5.83	5.59	4.41	4.86	5.5	20.31	12.15	
Pr	0.62	0.86	0.85	0.86	0.79	0.64	0.68	0.84	2.87	1.62	
Nd	3.45	4.70	4.36	4.56	4.35	3.61	3.59	4.22	16.45	8.34	
Sm	1.23	1.37	1.19	1.38	1.26	1.04	0.93	1.34	4.13	2.18	
Eu	0.75	0.93	1.06	1.10	0.98	0.77	0.64	0.70	2.07	1.76	
Gd	1.39	1.35	1.33	1.56	1.40	1.09	1.06	1.40	4.80	2.54	
Tb	0.29	0.27	0.26	0.28	0.27	0.23	0.20	0.26	0.67	0.39	
Dy	1.67	1.55	1.58	1.75	1.61	1.35	1.18	1.66	3.86	2.40	
Ho	0.39	0.31	0.31	0.31	0.32	0.26	0.24	0.31	0.69	0.45	
Er	0.94	0.94	0.92	0.95	0.95	0.82	0.66	0.90	2.02	1.47	
Tm	0.11	0.13	0.13	0.13	0.14	0.11	0.09	0.12	0.23	0.18	
Yb	0.73	0.84	0.79	0.84	0.80	0.71	0.59	0.84	1.55	1.35	
Lu	0.10	0.12	0.11	0.13	0.12	0.10	0.09	0.12	0.22	0.20	

Notes: LOI = loss on ignition, total iron reported as FeO^{total},* = estimated parental magma of lherzolite